Experimental investigation of the bond coat rumpling instability under isothermal and cyclic thermal histories in thermal barrier systems

By Rahul Panat and K. Jimmy Hsia*

Department of Theoretical and Applied Mechanics

University of Illinois, Urbana, IL 61801,USA

Abstract

Reliable life prediction models for the durability of thermal barrier coatings require the identification of the relative importance of various mechanisms responsible for the failure of the coatings at high temperatures. Studies of these mechanisms in sub-systems of thermal barrier coatings can provide valuable information. In the present work, we undertake an experimental study of "rumpling", or progressive roughening of the bond coat surface in the bond coat-superalloy systems upon high temperature exposure. Thermal cycling and isothermal experiments are carried out on a platinum-aluminide bond coat and on a NiCoCrAlY bond coat deposited on a Ni-based superalloy in air and in vacuum. The cyclic experiments are conducted in air from 200 °C to 1200 °C for different levels of initial roughness of the bond coat surfaces. Isothermal experiments are carried out at various temperatures, ranging from 960 °C to 1200 °C. The bond coat surfaces in cyclic experiments rumple to a similar characteristic wavelength of about 60-100 μm and an amplitude varying from 2 μm to 5 μm. Additional small scale fluctuations are seen to develop between the thermally grown oxide (TGO) and the bond coat surface with a wavelength of about 3-5 μm. Smooth initial bond coat surfaces (fluctuations in tens of nanometers) are seen to have rumpled, indicating that significant initial flaws are not required for rumpling to occur. Observations of the rumpled bond coat edges are shown to indicate that bond coat stresses play a dominant role during the rumpling process. On comparing the experimental observations with

*Corresponding author. Email: kj-hsia@uiuc.edu, Fax: 1(217) 244 5707.

existing rumpling models in literature, it is concluded that the TGO and the microstructural changes in the bond coat have a rather limited role in inducing rumpling. Diffusion driven by thermal mismatch stress in the bond coat is likely to be the dominant mechanism during rumpling.

Keywords: Thermal Barrier Coatings; Thermally activated process; Surface diffusion.

1 INTRODUCTION

Increasing demand for higher operating efficiencies of jet engines and gas turbines has led to the development of thermal barrier coating (TBC) technology over the last two decades (see Goward, 1998; Meier & Gupta, 1994; Miller, 1987; Padture *et al.*, 2002; Schulz *et al.*, 2003; Sheffler & Gupta, 1988; Stiger *et al.*, 1999; Strangman, 1985). The TBCs are multi-layered metal-ceramic coatings used to reduce the surface temperature of superalloy components in the hot sections of jet engines, gas turbines and diesel engines (e.g. Levy & MacAdam, 1988; Padture *et al.*, 2002; Rejda *et al.*, 1999). The higher operating temperatures made possible by TBCs result in higher engine efficiencies. For a fixed operating temperature, this translates into an improved oxidation resistance and prolonged creep life of the engine components. Anatomy of a typical TBC system consists of a ceramic topcoat, a thermally grown aluminum oxide (TGO), an intermediate (metallic) bond coat (BC) and a substrate superalloy. The BC is deposited on the superalloy, while the ceramic is deposited over the BC at high temperatures. The TGO is a reaction product that grows over the BC at high temperatures and occupies BC-ceramic interface. The BC is either platinum-aluminide or a NiCoCrAlY alloy.

In spite of the excellent advantages offered by TBCs, their long term durability is limited, primarily due to the problems associated with ceramic topcoat spallation. Since the local temperature in the hot section of a gas turbine can exceed the melting temperature of the superalloy, this spallation can be quite dangerous. Several laboratory and field experiments have been carried out in the past subjecting different types of TBC systems to failure under isothermal, thermomechanical or cyclic thermal histories (see Ambrico *et al.*, 2001; Bouhanek *et al.*, 2000; Ibegazene-Ouali *et al.*, 2000; Mumm *et al.*, 2001; Ruud *et al.*, 2001; Schulz *et al.*, 2001; Sohn *et al.*, 2001; Tolpygo & Clarke, 2001; Tolpygo *et al.*, 2001; Vaidyanathan *et al.*, 2000; Wright,

1998; Wu *et al.*, 1989). Although the TBC failure under thermal loading is seen to vary from system to system (e.g. Bouhanek *et al.*, 2000; Ruud *et al.*, 2001; Schulz *et al.*, 2001; Tolpygo & Clarke, 2001; Tolpygo *et al.*, 2001), some general trends can be established.

The most significant indication from these studies is that the failure process is associated with the morphological instabilities, or "rumpling", occurring at the BC-ceramic interface, with the TGO in between (from Evans *et al.*, 2001; Wright & Evans, 1999). Aspects of the rumpling phenomenon are explored in the past through experimental studies on TBC sub-systems consisting of the substrate coated with BC only (e.g., Deb *et al.*, 1987; Holmes & McClintock, 1990; Pennefather & Boone, 1995; Tolpygo & Clarke, 2000; Zhang *et al.*, 1999). Platinum aluminide and NiCoCrAlY BCs deposited on superalloy substrates rumple to wavelengths ranging from 30-50 μm (Tolpygo & Clarke, 2000) to about 300 μm (Pennefather & Boone, 1995) upon thermal cycling to temperatures up to 1200 °C. The amplitude of rumpled surface in these experiments was up to 15 μm. Under isothermal experiments at 1100 °C (Deb *et al.*, 1987) and at 1150 °C (Tolpygo & Clarke, 2000), no rumpling was observed. Under fast heating and cooling rates (1050°C to 300°C temperature change in about a minute) along with mechanical loading of the superalloy substrate, the BCs were seen to rumple (see Holmes & McClintock, 1990; Zhang *et al.*, 1999) with additional thermal shock effects such as "scalloping" (e.g. Holmes & McClintock, 1990), or large scale spallation of the TGO.

The critical question to understanding the failure process of TBC is: what are the mechanisms responsible for such rumpling of the BC-ceramic interface. Models for rumpling instabilities have been developed for generic metal-oxide systems (see He *et al.*, 2000; Suo, 1995), for specific BC-superalloy systems (see Tolpygo & Clarke, 2000), and for metallic coating-substrate systems (see Panat *et al.*, 2003) in which different mechanisms have been proposed to explain the experimental observations.

Some of these models emphasized the role played by the TGO. He *et al.* (2000) proposed that ratcheting of the BC due to the mismatch stresses in the developing TGO during thermal cycling is responsible for the rumpling. Such mechanism requires that the initial amplitude of surface fluctuation be larger than a critical value. Moreover, cyclic thermal history is a necessary condition for rumpling to occur. Suo (1995), on the other hand, suggested that the highly compressive stresses in the TGO (on the order of GPa) would provide the driving force necessary for the metal atoms to diffuse along the TGO-metal interface, leading to a wavy metal surface. Suo (1995)

estimates that this mechanism would result in a rumpling characteristic wavelength of a few times the thickness of TGO, roughly an order of magnitude smaller than that observed in experiments by Tolpygo & Grabke (1994). The mechanisms proposed by He *et al.* (2000) and by Suo (1995) are generic for all metal-oxide systems. Other models concern the microstructural changes in the BC during high temperature testing. Based on their experimental observations, Tolpygo & Clarke (2000) suggested that the rumpling in BC-superalloy systems occurs as a result of diffusion of various constituents, like Ni and Al, perpendicular to the BC surface. In order to verify this mechanism, however, one needs to quantitatively demonstrate the correlation between microstructural features, such as composition variations, and surface rumpling features. Recently, Panat *et al.* (2003) developed a model based on the assumption that the stress in BC is the driving force for the BC surface atoms to diffuse, and will give rise to rumpling with characteristic wavelengths decided by the energetics of the process, i.e. a balance between strain energy and surface energy of the BC. Among all the mechanisms proposed by the above models, it is unclear, from the experimental data available to date, which mechanism (or mechanisms) is dominant during the rumpling process.

Present work is inspired by the experimental observations of BC surface rumpling (see Deb *et al.*, 1987; Holmes & McClintock, 1990; Pennefather & Boone, 1995; Tolpygo & Clarke, 2000; Zhang *et al.*, 1999) and theoretical predictions by various models (e.g. He *et al.*, 2000; Panat *et al.*, 2003; Suo, 1995; Tolpygo & Clarke, 2000), and tries to shed light on the issue. A detailed experimental study of the rumpling of BC-superalloy system subjected to isothermal and cyclic thermal heat treatments in air is performed. Both platinum aluminide and NiCoCrAlY bond coated superalloy are considered. The results demonstrated that rumpling of similar patterns occurs under a wide range of conditions such as isothermal and thermal cycling with drastically different initial surface fluctuations. An experiment of a platinum aluminide BC subjected to an isothermal condition in vacuum is also presented. This result shows that the rumpling can occur in absence of significant TGO. Microstructural examinations reveal poor correlation between microstructural changes and rumpling peak/valley locations. At the temperatures used in this study, experimental results indicate that the mechanism proposed by Panat *et al.* (2003), i.e., rumpling driven by BC mismatch stress, is likely to be responsible for the observed rumpling behavior. Findings in the current work point to the need of 'mechanism maps' showing the dominant mechanisms active in thermal barrier systems at various temperatures and

times.

2 EXPERIMENTAL PROCEDURE

The substrate material used in the BC-superalloy systems in the current study was René N5, a Ni-based superalloy provided by General Electric Aircraft Engines (Cincinnati, OH). The superalloy samples were 5 mm × 5 mm × 22 mm in dimension. One of the surfaces of these samples was polished successively down to 1 μm diamond paste to remove initial surface roughness prior to BC deposition. Two types of BC materials, NiCoCrAlY and platinum aluminide were deposited on the superalloy by Chromalloy Gas Turbine Corporation (Orangeburg, NY). The platinum aluminide BC was deposited by electroplating a Pt layer followed by a vacuum heat treatment at 927 °C. Finally, a vapor phase aluminization at 1080 °C completed the deposition process. The NiCoCrAlY BC was deposited by the electron beam physical vapor deposition (EB-PVD) method. Each of the BC-superalloy samples were cut further using a wafering blade (Buehler, Lake Bluff, IL) into cubes of approximately 5 mm × 5 mm × 5 mm. During the cutting process, each sample was protected by embedding it in an acrylic mount. The mount was then removed by acetone.

To observe the effect of surface texture on rumpling, three types of surface morphologies were induced on each type of the BC surfaces. In the first type, the BC surface was polished successively down to 1 μm diamond paste to produce a highly smooth surface. The second and the third type of the BC surfaces were polished by 60 grit and 600 grit SiC papers (Buehler, Lake Bluff, IL). In case of the platinum aluminide BC, an as-deposited surface was also used for comparison. The specimens were subjected to thermal cycling or isothermal heat in air. The thermal cycles, 25 in number, consisted of heating the specimens to 1200 °C in 55 minutes, a hold time of about 50 min at 1200 °C, followed by air cooling to 200 °C in 25 minutes. Isothermal experiments were carried out on platinum-aluminide BC at 960 °C, 1100 °C, and 1175 °C with a hold time of 100 hours and also at 1200 °C with a hold time of 25 hours. The hold time at 1200 °C was chosen so as to be approximately equal to the total time at high temperature for the cyclic experiments. The choice of the other temperatures and hold times for isothermal experiments is explained in § 4. A specimen with platinum aluminde BC was also subjected to isothermal exposure at 1200 °C for 25 hours in vacuum (about 10^{-5} torr) environment. For uniformity, the surfaces of all the BC samples used in isothermal experiments were polished successively down

to 1 μm diamond paste.

A box furnace (Vulcan 3-400HTA, NEYTECH, Bloomfield, CT) was used to carry out all the experiments in air. A tube furnace (HTF55322A, Lindberg/Blue M, Asheville, NC) along with a quartz tube was used to carry out the experiment in vacuum environment. The quartz tube that carried the specimens ran through the tube furnace. The tube was connected to a roughing pump/diffusion pump assembly to produce a vacuum of about 10^{-5} torr. Temperature during the experiments was measured using a K-type thermocouple (Omega, Stamford, CT). Some of the samples were cut and their cross section polished successively down to 1 μm diamond paste to observe the microstructural changes. The samples were examined using scanning electron microscopy (SEM), the semi quantitative elemental analysis tool of energy dispersive X-ray spectroscopy (EDX), and profilometry.

3 EXPERIMENTAL RESULTS

3.1 Initial Microstructure and Composition

Representative SEM images of the two types of BCs are shown in Fig. 1. Figure 1a shows the cross-section of the platinum aluminide BC having an outer zone (region 1) and an interdiffusion zone (IDZ) (region 2). The nominal composition of the BC is (wt%) 17Al-3.4Cr-5.9Co-34Pt-bal Ni as determined by EDX analysis. The BC is β-Ni(Pt)Al with the IDZ containing precipitates (bright regions in Fig. 1a) rich in refractory elements (W, Mo, and Ta). Alumina inclusions, shown by black arrows in Fig. 1a, were regularly placed at the border between region 1 and region 2. Occasionally, pores were observed in region 1 as indicated by the white arrow in Fig. 1a. This structure is typical of the platinum aluminide coatings reported in literature (Deb *et al.*, 1987; Mumm *et al.*, 2001; Tolpygo & Clarke, 2000). The BC composition in the outer zone varied slightly in the direction perpendicular to the BC surface. Towards the top, the Al content increases (about 22 wt%), while towards the IDZ, the Al content decreases (about 15 wt%) with a concomitant increase in Co and Cr content. The nominal thickness of the IDZ was about 22$\pm$2 μm, while the thickness of the outer zone varied from about 24 to 30 μm depending upon the polishing treatment of the surface. A possible effect of this variation on the rumpling behavior is discussed in §4. Figure 1b shows a SEM micrograph (with backscatter electrons) of top surface of the platinum aluminide BC polished successively down to 1 μm diamond paste. The

BC grains of about 10 μm size are seen with occasional occurrences of larger grains of 15-20 μm size. The grain boundaries in Fig. 1b show bright regions representing secondary $PtAl_2$. These regions were present near the surface, reducing successively for thinner outer zones. Figures 1(c,d) show cross-section images of a NiCoCrAlY BC at different magnifications. The randomly distributed dark and bright regions in Fig. 1d represents regions with an Al content of about 4 wt% and 15 wt%, respectively. The composition of the René N5 superalloy can be found in Walston *et al.* (1996).

3.2 Rumpling Observations

3.2.1 Thermal cycling Experiments

Representative SEM micrographs of initial and rumpled surfaces of platinum aluminide BC under 25 thermal cycles from 200 °C to 1200 °C, along with the profilometer scans are shown in Figs. 2(a-d). The profilometer scans in Figs. 2(a2,b2,a4,b4,c2,d2,c4,d4) correspond to the BC surfaces shown in Figs. 2(a1,b1,a3,b3,c1,d1,c3,d3), respectively. All scans have the same scale along the vertical axis for comparison. Further, the scan lengths have been chosen to be identical to the actual width of the SEM pictures. Figure 2a1 shows a BC surface polished successively down to 1 μm diamond paste, while Figs. 2(b1,c1,d1) show BC surfaces polished with 600 grit SiC paper, with 60 grit SiC paper and in an as-deposited condition, respectively. The corresponding line scans in Figs. 2(a2,b2,c2,d2) show surface fluctuations with a peak-to-valley distance of about 0.02 μm (not seen at the scale shown), 0.25 μm, 3 μm and 2.5 μm, respectively. On subjecting these samples to 25 thermal cycles, the BC surfaces develop waviness as seen in Figs. 2(a3,b3,c3,d3) with peak-to-valley distance of about 4-5 μm, 10 μm, 6 μm and 8 μm, respectively. Note that the scans for the BC surfaces polished with SiC grit (Figs. 2(b1,c1)) are perpendicular to the polishing direction. The characteristic wavelengths of the rumples for all the samples can be seen to be about 60-100 μm. It is interesting to see that the amplitudes of the initial waviness of the BC samples varied over two orders of magnitude, while those after thermal cycling were of the same order of magnitude. Figures 2(a1-4) indicate that significant initial defects on the BC surface were not needed for rumpling to occur. Further, the rumpling pattern seen in Figs. 2(b3,c3) does not appear to be influenced by the initial scratching directionality of the corresponding BC surfaces, Figs. 2(b1,c1). The rumples on the BC surface are randomly oriented, but have some local directionality.

Cross-sectional examination of the rumpled BC revealed additional important features of the rumpling phenomenon. Figure 3 is a cross-sectional SEM image of the rumpled surface in Fig. 2a3. The higher magnification image in Fig. 3 reveals a 1-2 μm thick TGO layer formed over the BC. The TGO is non-uniform in thickness due to a wavy BC-TGO interface. The wavelength of this interfacial waviness is about 3-5 μm, while its amplitude is slightly less than a micron. Thus, the BC top surface has a smaller waviness with a characteristic wavelength a few times the TGO thickness.

The platinum aluminide BC also experienced changes in the initial microstructure upon thermal cycling as seen from the SEM image (with backscatter electrons) in Fig. 4, although the presence of two distinct regions in the cross section was similar to that before cycling as seen in Fig. 1a. The upper region has BC grain boundaries with intermittent regions of Al depleted γ' phase (Fig. 4b) not seen in Fig. 1. The Al depletion can also be seen at the β grain boundaries in Fig. 4. The depleted Al is believed to be utilized in the formation of the TGO (see He *et al.*, 2000; Holmes & McClintock, 1990; Tolpygo & Clarke, 2000) during thermal cycling. The lower region of the cross section (Fig. 4a) can be seen to have randomly distributed (bright) precipitates rich in W, Mo and Ta. Comparing with the initial microstructure in Fig. 1a, it is seen that the precipitates have undergone considerable coarsening and agglomeration upon high temperature exposure. Note that the apparent thickness of the BC has considerably increased upon thermal cycling, consistent with the observations in the past (e.g. He *et al.*, 2000; Holmes & McClintock, 1990). This increase is believed to be due to diffusion of Ni from the superalloy to the BC at high temperature and the subsequent decrease of the solubility of refractory elements below the BC-substrate interface (Holmes & McClintock, 1990).

An interesting rumpling pattern was observed near the free edge of the specimens. Figure 5a is an SEM micrograph of the middle region of a rumpled sample showing the random distribution of surface undulations. At the free edge, however, the rumpling ridges are distinctly aligned perpendicular to the edge as shown in Fig. 5b. As shown schematically in Fig. 5c, the tensile stress normal to the free edge, σ_{xx}, in the BC vanishes at the edge. This stress component will gradually build up to the maximum over a distance of the order of the film thickness. In Fig. 5b, both the TGO and the BC are stress free at the edge. The extent of the 'edge zone' is, however, of the order of the BC thickness (≈ 100 μm).

Rumpling results for the NiCoCrAlY bond coat-superalloy system upon thermal cycling are shown in Figs. 6(a-d). The NiCoCrAlY BC surface polished down to 1

μm diamond paste is shown in Figs. 6(a,b). It is seen in Fig. 6(c,d) that, upon 25 thermal cycle, the BC surface rumples at a wavelength about the same as that of the platinum aluminide BC. The peak-to-valley distance in the initial waviness in Figs. 6(a,b) is about 50 nm (not seen for the scale shown in the figure). The rumple amplitude of the NiCoCrAlY BC (Fig. 6d) is about 2 μm, smaller than that for the platinum aluminide BC (Figs. 2(a3,a4)) by about a factor of two. For the NiCoCrAlY BC surface polished by 600 and 60 grit SiC paper, the initial surface fluctuations were too large for the rumpling to be observed.

3.2.2 Isothermal Experiments in air

Figure 7 shows a representative SEM micrograph and the corresponding profilometer scan of the surface of a platinum aluminide BC-superalloy specimen subjected to 1200 °C isothermal exposure for 25 hours. As seen in Fig. 7b, the BC under isothermal exposure has rumpled with comparable rumpling amplitude and wavelength as that under thermal cycling experiments seen in Fig. 2a4. A representative SEM micrograph with backscatter electrons of the cross-section of the BC subjected to 1200 °C isothermal exposure for 25 hours is shown in Fig. 8. Similar to the thermally cycled samples seen in Fig. 4, the BC for the isothermal experiments can be divided roughly into two regions, an upper region showing grain boundaries and a lower region consisting of bright precipitates rich in W, Mo and Ta. However, unlike the thermally cycled samples, the γ' transformation regions were not seen in the upper region after isothermal treatment in Fig. 8. Figure 8 also shows alumina inclusions as dark regions at the boundary of the outer and the inner region of the BC. These alumina inclusions were present before the isothermal exposure as seen in Fig. 1a.

The rumpled surfaces seen in Figs. 7a, 2a3 and 2b3 all have a waviness with comparable wavelength and amplitude, but they appear to have a different degree of local directionality. The cause of the local directionality in rumpling patterns and its variation is not clear at present. A similar observation has been made by Tolpygo & Clarke (2000) for systems subjected to thermal cycling. Rumpling similar to that in Fig. 7 is observed in specimens under 1175 °C isothermal exposure for 100 hours in Fig. 9a. But for isothermal experiments at 1100 °C and 960 °C with a hold time of 100 hours, no apparent rumpling could be observed (Fig. 9(b,c)). In case of isothermal exposure at 1175 °C for 100 hours, the BC developed voids, about 10-15 μm across near the interface between the upper and the lower regions, Fig. 10. These voids were irregularly placed at a distance ranging from 90 μm to 1 mm from each other. An

isolated void was observed at 1200 °C after 25 hours, while at other temperatures, isothermal exposure did not result in void formation.

3.2.3 Isothermal Experiments in Vacuum

Figure 11 shows the result from the experiment conducted at 1200 °C for 25 hours in vacuum. The initial BC surface was polished successively down to 1 μm diamond paste similar to that in Figs. 2(a1,a2). From the SEM micrograph and the corresponding profilometer scan in Fig. 11, it can be seen that the BC surface has rumpled upon isothermal exposure. The TGO thickness over this BC surface was estimated to be less than 10 nm from X-ray photoelectron spectroscopy (XPS) studies. Note from Figs. 2 and 11 that the rumple wavelengths and amplitudes in the vacuum experiment are comparable to those in air.

4 DISCUSSION

The experimental results presented in the current work elucidate several aspects of the rumpling phenomenon. It is shown that rumpling of the BC surfaces can occur under cyclic as well as isothermal temperature histories. Bond coat surfaces with vastly different initial surface morphologies are shown to have rumpled to comparable wavelengths and amplitudes upon thermal cycling. Changes in the microstructure of the BC have been observed during rumpling. In the present section we analyze these results in the context of the existing rumpling models by He *et al.* (2000), Suo (1995), Tolpygo & Clarke (2000), and Panat *et al.* (2003) to draw conclusions regarding the possible rumpling mechanisms.

4.1 Role of TGO in Inducing BC Rumpling

Figure 12 shows SEM micrographs of a superalloy specimen without the BC subjected to identical thermal cycles as those with the BC shown in Fig. 3. The micrographs at different magnifications (Fig. 12(a,b)), show that the superalloy surface has not rumpled in spite of the fact that the TGO on the superalloy surface is thicker than that on the BC surface (see Fig. 3). Prior to thermal cycling, the superalloy surface in Fig. 12 was polished successively down to 1 μm diamond paste, similar to that in Fig. 2(a1,a2). The supralloy surface exposed due to chipping of the TGO (Fig. 12b) has developed a surface roughness during thermal cycling. Note that the TGO

spallation seen in Fig. 12b occurred during cutting of the specimen after the thermal cycling experiment.

Under thermal cycling of the bulk superalloy, the TGO stresses alone are expected to be dominant; while for the BC on the superalloy, the stresses in both the BC and the TGO might be important. Figure 12 demonstrates that the presence of BC is critical for the rumpling to occur. Moreover, we observed from Fig. 2 that initial flaws of certain amplitude were not necessary to cause the BC surface to rumple, as required by the TGO driven ratcheting model of He *et al.* (2000). These experiments suggest that the role of the TGO is limited in inducing the long range rumpling seen in the present work and previous studies (e.g. Deb *et al.*, 1987; Holmes & McClintock, 1990; Pennefather & Boone, 1995; Tolpygo & Clarke, 2000; Zhang *et al.*, 1999).

In fact, TGO of a few microns thickness is not likely to result in rumpling with wavelengths of the order of 100 μm. Similar inference has been drawn by Suo (1995) and also by Tolpygo & Clarke (2000). Suo (1995) suggests that his TGO stress driven diffusion model (Suo, 1995) coupled with TGO growth kinetics would cause a metal substrate to rumple with wavelengths a few times the TGO thickness (e.g. Tolpygo & Grabke, 1994). Note that the small scale waviness observed in the present work (Fig. 3) has indeed a wavelength that is a few times the TGO thickness. Tolpygo & Clarke (2000) have reported that significant difference in the levels of TGO stresses at room temperature has no quantitative effect in the resulting BC rumpling amplitudes and wavelengths, further indicating limited role of TGO in determining the rumpling behavior.

A further confirmation of this inference can be seen in the rumpling observed in Fig. 11 under vacuum environment. The TGO with a thickness less than 10 nm over this BC surface cannot possibly be the cause of BC rumpling to the wavelengths seen in Fig. 11. Figures 2 and 11 show that the rumpling wavelengths and amplitudes in the vacuum experiment are comparable to those in air, confirming again that TGO is not needed to induce the long range rumpling. For thicker TGOs developed in these systems and for soft substrates (see Karlsson & Evans, 2001), the TGO may play an important role in the system behavior. The role of the TGO growth stresses in the development of the small scale waviness observed in the current experiments (Fig. 3) needs further work.

4.2 Role of BC Microstructural Changes in inducing BC Rumpling

Tolpygo & Clarke (2000) suggested that the rumpling behavior is related to the microstructural changes in the BC. Particularly, the roles of the γ' phase formed in the BC under cyclic oxidation and the voids formed in the BC under isothermal oxidation have been emphasized. It was suggested that rumpling and void formation may be different manifestations of some form of a common volume depletion process. To check the validity of this argument, we analyzed Fig. 4 for a possible correlation between the microstructural evolution and BC rumpling behavior. Figure 13 shows the number of occurrences of the γ' phase in the BC cross-section in Fig. 4a, as a function of their relative location with respect to the rumple peak and the adjacent rumple valley. If the distance between a peak and the nearest γ' region is S_i, the normalized distance l_i is calculated by

$$l_i = 2\left(\frac{S_i}{\lambda_i}\right) \tag{1}$$

where λ_i is the wavelength of the surface undulation at the occurrence of the γ' phase as shown in Fig. 13. It is clear that the γ' phase coincides with the peak when the normalized distance $l \approx 0$, or with the valley when $l \approx 1$. Figure 13 shows that the γ' phase is not preferentially oriented either towards the valleys or towards the peaks of the rumples. A further look at Fig. 4 reveals that the occurrence of bright regions representing the precipitates rich in W, Mo and Ta have a poor correlation with the occurrence of the rumples. The grain boundaries of the rumpled BC grains seen in Fig. 4 do not show a tendency to be either towards the peaks or towards the valleys of rumples. Note also that prior to thermal cycling, the microstructural periodicity associated with the precipitates in the IDZ of the platinum aluminide BC is about 2-3 μm (Fig. 1a), while that associated with the bright and dark regions in NiCoCrAlY BC, is about 3-4 μm (Fig. 1d); much smaller than the rumple wavelengths seen in experiments (Figs. 2 and 6). These observations indicate that the microstructural changes occurring in the BC are not strongly correlated to the rumpling phenomenon. A study of TBC systems by Mumm *et al.* (2001) with a similar BC as in the present work has also shown a poor correlation between occurrence of γ' domains and BC instability sites (i.e. valleys in presence of the ceramic topcoat) in their experiments.

Furthermore, the isothermal experimental results at 1175 °C shown in Figs. 9a and 10 indicate the distance between these voids (90 μm to 1 mm) did not correspond well with the rumple wavelength. It should be recognized that void formation under

isothermal conditions is an important phenomenon that can influence TBC failure (e.g. Tolpygo & Clarke, 2001). However, the relationship between BC rumpling and void formation is not well established.

4.3 BC Stress Driven Surface Diffusion Mechanism

In this section, the observations of the rumpling behavior are compared with the BC stress driven surface diffusion mechanism proposed by Panat *et al.* (2003). The model by Panat *et al.* (2003) has several implications as a result of the proposed mechanism. One implication is that the rumpling behavior should be relatively insensitive to the initial surface fluctuations as long as the amplitudes of the initial fluctuations are significantly smaller than the thickness of the BC. Our experimental observations shown in Fig. 2 demonstrate that vastly different initial surfaces with roughness from tens of nanometers to a few microns will all evolve into similar rumpled surfaces upon thermal cycling. Moreover, as mentioned in §3.2.1, the extent of the "edge zone", in which the rumpling ridges are aligned perpendicular to the stress-free edge, is consistent with the mechanism that the rumpling is driven by a stress in the BC. The model by Panat *et al.* (2003), using estimates of material parameters from literature (Freund, 1995; Karlsson & Evans, 2001), predicts that the characteristic wavelength of the rumpled surfaces is about 100-250 μm, which is also consistent with the measured rumpling wavelengths in the present work as well as in other researchers' observations (namely, Deb *et al.*, 1987; Holmes & McClintock, 1990; Pennefather & Boone, 1995; Tolpygo & Clarke, 2000; Zhang *et al.*, 1999).

The source of stresses in the BC is the thermal mismatch strain due to the difference in thermal expansion coefficients between the BC and the substrate materials. As a result, the model by Panat *et al.* (2003) does not discriminate between cyclic thermal and isothermal histories. As long as the temperature is sufficiently different from the BC processing temperature such that enough mismatch stress exists in the BC, rumpling will occur. Indeed, our experiments show that, under isothermal conditions at 1200 °C and 1175 °C in air and at 1200 °C in vacuum, BC surface rumpling occurs with similar amplitudes and wavelengths as those subjected to cyclic thermal history. However, our isothermal experiments at 1100 °C and 960 °C for 100 hours did not result in any rumpling of the BC surface, neither did Tolpygo & Clarke's (2000) isothermal experiment at 1150 °C. Using the model by Panat *et al.* (2003), we estimated the time required, at different isothermal heating temperatures, to generate the waviness of the same magnitude as that subjected to 1200 °C exposure. The

result is shown in Fig. 14. The biggest uncertainty in generating this figure is the BC processing temperature, i.e., the "stress-free temperature". Based on the fact that a vapor phase aluminization was conducted at 1080 °C following a heat treatment at 927 °C for our specimens, we considered several processing temperatures in Fig. 14. The solid symbols indicate that rumpling has occurred, whereas open symbols indicate no rumpling. Fig. 14 shows that, if the processing temperature is about 1050 °C, rumpling will occur after 25 hours exposure at 1200 °C and after 100 hours at 1175 °C. However, for the BC surface to generate a comparable rumpling at 1150 °C, approximately 780 hours of heating time is needed, substantially longer than the exposure time used by Tolpygo & Clarke (2000). The exposure times of our isothermal experiments at 1100 °C and 960 °C as well as other researchers' experiment at 1100 °C (see Deb *et al.*, 1987) are all far shorter than what is needed to produce reasonable rumpling of BC surface. It should also be pointed out that, in generating Fig. 14, we assumed that the specific diffusivity D_0 and the activation energy q for surface diffusion in the BC remain constant at all temperature levels, which may not be true, especially at lower temperatures.

Recently, Suo *et al.* (2003) have found that after 300 hours exposure at 1150 °C, the BC develops extensive voids near the surface. The void formation was attributed to the diffusion of BC constituents perpendicular to the BC top surface (Suo *et al.*, 2003). Clearly, void formation appears to dominate the BC behavior at 1150 °C after a long time. It is conceivable that at different temperatures, different mechanisms may be dominant during high temperature exposure. We are currently conducting isothermal experiments in vacuum and in air to identify whether the stress driven surface diffusion is the dominant mechanism below the processing temperature. The choice of testing temperatures and exposure durations will be guided by the stimates presented in Fig. 14. Extensive experimental observations are needed to obtain a 'mechanism map' in these systems. Such a map can predict their behavior under different conditions and can ultimately be used to enhance their performance in TBCs.

5 CONCLUSIONS

In the present work, isothermal and cyclic thermal experiments are carried out on BC-superalloy systems. The results indicate that:

- Rumpling can occur under both thermal cycling and isothermal heating conditions.

- Rumpling wavelength is relatively insensitive to initial BC surface fluctuations. Significant initial flaws are not needed for rumpling to occur.
- TGO plays a limited role in BC surface rumpling behavior. Rumpling occurs even in the absence of oxidation when experiments are conducted in vacuum.
- Several microstructural changes occur in the BC during rumpling. These changes are found to have a poor correlation with the periodicity associated with rumpling.
- Rumpling behavior under isothermal conditions depends upon the hold temperature and time.
- At temperatures above the processing temperature, BC stress driven surface diffusion (Panat *et al.*, 2003) is likely to be the dominant mechanism for rumpling.

Acknowledgement

The work is supported by a Critical Research Initiative program at the University of Illinois at Urbana-Champaign (UIUC). Thanks go to Dr. Ram Darolia of General Electric for providing the superalloys. Thanks also go to the Paul Lawton, Stacy Fang, and Anthony Collucci of Chromally, NY for coating the superalloys with the bond coat. The SEM, XRD and profilometry work was carried out in the Center for Microanalysis of Materials, Frederick Seitz Materials Research Laboratory, UIUC, which is partially supported by the U.S. Department of Energy under grant DEFG02-91-ER45439. The authors would like to acknowledge helpful discussions with Prof. T.-C. Chiang, Dr. Sulin Zhang and Ming Liu at UIUC.

References

Ambrico, J. M., Begley, M., & Jordan, E. H. 2001. Stress and shape evolution in oxide films on elastic-plastic substrates due to thermal cycling and film growth. *Acta Mater.*, 1577-1588, 49–52.

Bouhanek, K., Adesanya, O. A., Stott, F. H., Skeldon, P., Lees, D. G., & Wood, G. C. 2000. Isothermal and thermal cyclic oxidation behavior of thermal barrier coatings: Pt aluminide bond coat. *Mat. High Temp.*, 2, 185–196.

Deb, P., Boone, D. H., & Manley, T. F. I. 1987. Surface instability of platinum modified aluminized coatings during 1100 °C cyclic testing. *J. Vac. Sci. Technol.*, 5(6), 3366–3372.

Evans, A. G., Mumm, D. R., Hutchinson, J. W., Meier, G. H., & Pettit, F. S. 2001. Mechanisms controlling the durability of thermal barrier coatings. *Prog. Mat. Sci.*, 46, 505–553.

Freund, L. B. 1995. Evolution of waviness on the surface of a strained elastic solid due to stress-driven diffusion. *Int. J. Sol. Struct.*, 32(6-7), 911–923.

Goward, G. W. 1998. Progress in coatings for gas turbine airfoils. *Surf. Coat. Technol.*, 108-109, 73–79.

He, M. Y., Evans, A. G., & Hutchinson, J. W. 2000. The ratcheting of compressed thermally grown thin films on ductile substrates. *Acta Mater.*, 48, 2593–2601.

Holmes, J. W. & McClintock, F. A. 1990. The chemical and mechanical processes of thermal fatigue degradation of an aluminide coating. *Metall. Trans.*, 21A, 1209–1222.

Ibegazene-Ouali, F., Mervel, R., Rio, C., & Renollet, Y. 2000. Microstructural evolution and degradation modes in cyclic and isothermal oxidation of an EB-PVD thermal barrier coating. *Mat. High Temp.*, 17, 205–218.

Karlsson, A. M. & Evans, A. G. 2001. A numerical model for the cyclic instability of thermally grown oxides in thermal barrier coatings. *Acta Mater.*, 49, 1793–1804.

Levy, A. V. & MacAdam, S. 1988. Durability of ceramic coatings in 14,000 hours service in a marine diesel engine. *ASME Paper*, pp. No.88–ICE–19.

Meier, S. M. & Gupta, D. K. 1994. The evolution of thermal barrier coatings in gas turbine engine applications. *J. Eng. Gas Turbine Power*, 116, 250–257.

Miller, R. A. 1987. Current status of thermal barrier coatings-an overview. *Surf. Coat. Technol.*, 30, 1–11.

Mumm, D. R., Evans, A. G., & Spitsberg, I. T. 2001. Characterization of a cyclic displacement instability for a thermally grown oxide in a thermal barrier system. *Acta Mater.*, 49, 2329–2340.

Padture, N. P., Gell, M., & Jordan, E. H. 2002. Thermal barrier coatings for gas-turbine engine applications. *Science*, 296, 280–284.

Panat, R. P., Zhang, S., & Hsia, K. J. 2003. Bond coat surface rumpling in thermal barrier coatings. *Acta Mater.*, 51, 239–249.

Pennefather, R. C. & Boone, D. H. 1995. Mechanical degradation of coating system in high-temperature cyclic oxidation. *Surf. Coat. Technol.*, 76-77, 47–52.

Rejda, E. F., Socie, D., F., & Itoh, T. 1999. Deformation behavior of plasma-sprayed thick thermal barrier coatings. *Surf. Coat. Technol.*, 113, 218–226.

Ruud, J. A., Bartz, A., Borom, M. P., & Johnson, C. A. 2001. Strength degradation and failure mechanisms of electron-beam-physical-vapor-deposited thermal barrier coatings. *J. Am. Ceram. Soc.*, 84(7), 1545–1552.

Schulz, U., Leyens, C., Fritscher, K. andPeters, M., Saruhan-Brings, B., Lavigne, O., Dorvaux, J., Poulain, Mevrel, R., & Calez, M. 2003. Some recent trends in research and technology of advanced thermal barrier coatings. *Aero. Sci. Technol.*, in press.

Schulz, U., Menzebach, M., Leyens, C., & Yang, Y. Q. 2001. Influence of substrate material on oxidation behavior and cyclic lifetime of EB-PVD TBC systems. *Surf. Coat. Technol.*, 146-147, 117–123.

Sheffler, K. D. & Gupta, D. K. 1988. Current status and future trends in turbine applications of thermal barrier coatings. *J. Eng. Gas Turbine Power*, 110, 605–609.

Sohn, Y. H., Kim, J. H., Jordan, E. H., & Gell, M. 2001. Thermal cycling of EB-PVD/MCRALY thermal barrier coatings: I. microstructural development and spallation mechanisms. *Surf. Coat. Technol.*, 146-147, 70–78.

Stiger, M. J., Yanar, N. M., Topping, M. G., Pettit, F. S., & Meier, G. H. 1999. Thermal barrier coatings for the 21st century. *Z. Metallkd.*, 90(12), 1069–1078.

Strangman, T. E. 1985. Thermal barrier coatings for turbine airfoils. *Thin Solid Films*, 127, 93–106.

Suo, Z. 1995. Wrinkling of the oxide scale on an aluminium-containing alloy at high temperatures. *J. Mech. Phys. Solids*, 43(6), 829–846.

Suo, Z., Kubair, D., Evans, A. G., Clarke, D. R., & Tolpygo, V. 2003. Stresses induced in alloys by selective oxidation. *Acta Mater.*, 51, 959–974.

Tolpygo, V. K. & Clarke, D. R. 2000. Surface rumpling of a (Ni,Pt)Al bond coat induced by cyclic oxidation. *Acta Mater.*, 48, 3283–3293.

Tolpygo, V. K. & Clarke, D. R. Damage induced by thermal cycling of thermal barrier coatings. In Dahotre, N. B., Hampikian, J. M., & Morral, J. E., ed., *Elevated Temperature Coatings: Science & Technology IV*, pp. 94. TMS, 2001.

Tolpygo, V. K., Clarke, D. R., & Murphy, K. S. 2001. Oxidation induced failure of EB-PVD thermal barrier coatings. *Surf. Coat. Technol.*, 146-147, 124–134.

Tolpygo, V. K. & Grabke, H. J. 1994. Microstructural characterization and adherence of the α-Al_2O_3 oxide scale on the Fe-Cr-Al and Fe-Cr-Al-Y alloys. *Oxid. Met.*, 41, 343–2601.

Vaidyanathan, K., Gell, M., & Jordan, E. 2000. Mechanisms of spallation of electron beam physical vapor deposited thermal barrier coatings with and without platinum aluminide bond coat ridges. *Surf. Coat. Technol.*, 133-134, 28–34.

Walston, W. S., O'Hara, K. S., Ross, E. W., Pollock, T. M., & Murphy, W. H. René N6: Third generation single crystal superalloy. In Kissinger, R. D., Deye, D. J., Anton, D. L., Cetel, A. D., Nathal, M. V., Pollock, T. M., & Woodford, D. A., ed., *Proc. Superalloys Symp.*, pp. 27–33. The Minerals, Metals & Materials Society (TMS), 1996.

Wright, P. K. 1998. Influence of cyclic strain on life of a PVD TBC. *Mat. Sci. Engng.*, A245, 191–200.

Wright, P. K. & Evans, A. G. 1999. Mechanisms governing the performance of thermal barrier coatings. *Curr. Op. Sol. St. & Mat. Sci.*, 4, 255–265.

Wu, B. C., Chang, E., Chang, S. F., & Chao, C. H. 1989. Thermal cyclic response of yttria-stabilized zirconia/CoNiCrAlY thermal barrier coatings. *Thin Solid Films*, 172, 185–196.

Zhang, Y. H., Withers, P. J., Fox, M. D., & Knowles, D. M. 1999. Damage mechanisms of coated systems under thermomechanical fatigue. *Mat. Sci. Technol.*, 15, 1031–1036.

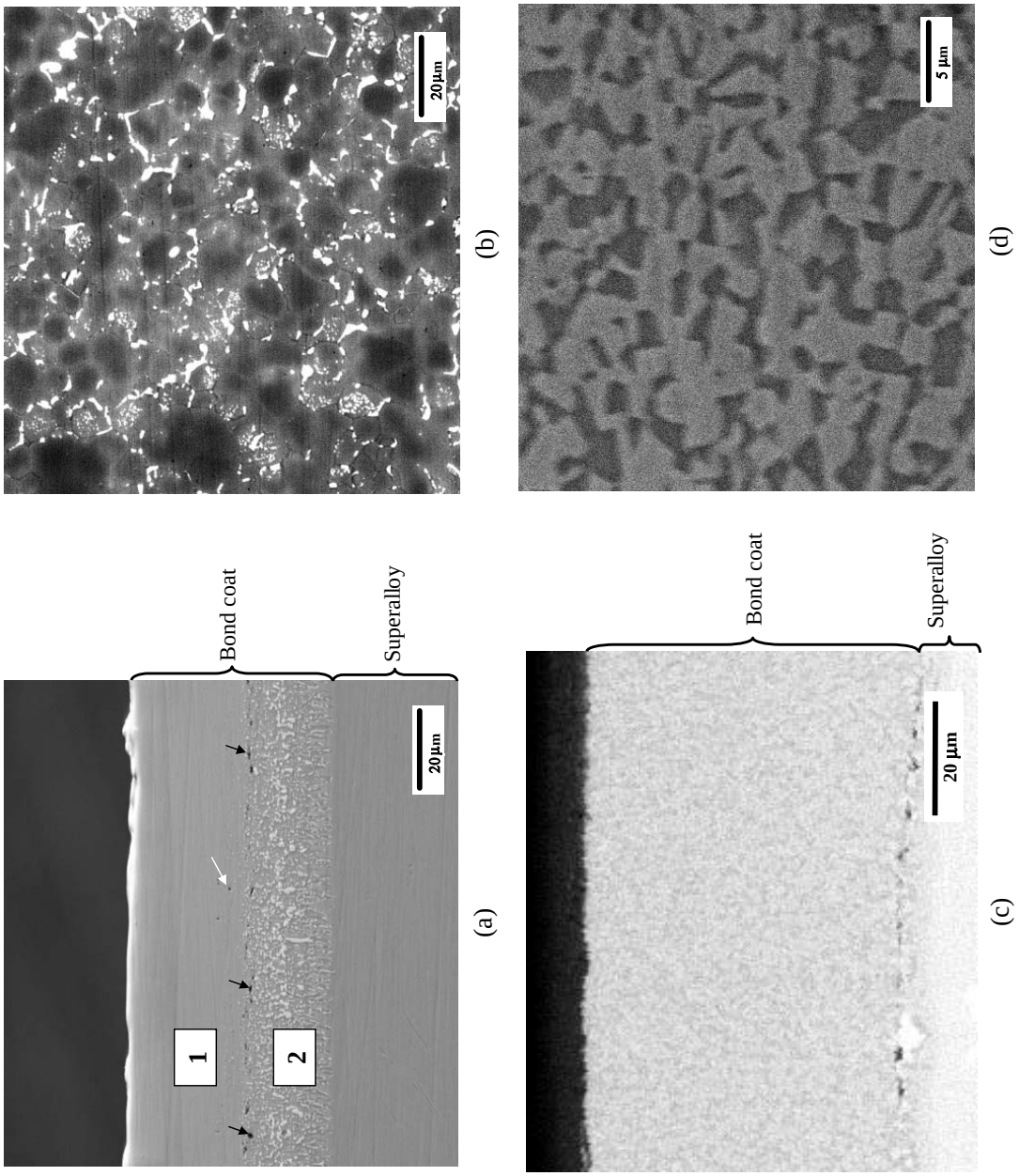

Figure 1: Bond coat microstructures prior to thermal cycling. (a) Cross-sectional SEM micrograph of platinum aluminide BC showing outer zone (label '1') and interdiffusion zone (label '2'). Black arrows show alumina inclusions regularly placed between the two regions, while the white arrow shows a pore seen intermittently in the outer region. (b) SEM micrograph (with backscatter electrons) of platinum aluminide BC top surface polished to 1 μm diamond paste. (c,d) SEM images of NiCoCrAlY BC cross section at different magnifications. The randomly distributed dark and bright regions in (d) represent regions with an Al content of about 4 wt% and 15 wt%, respectively.

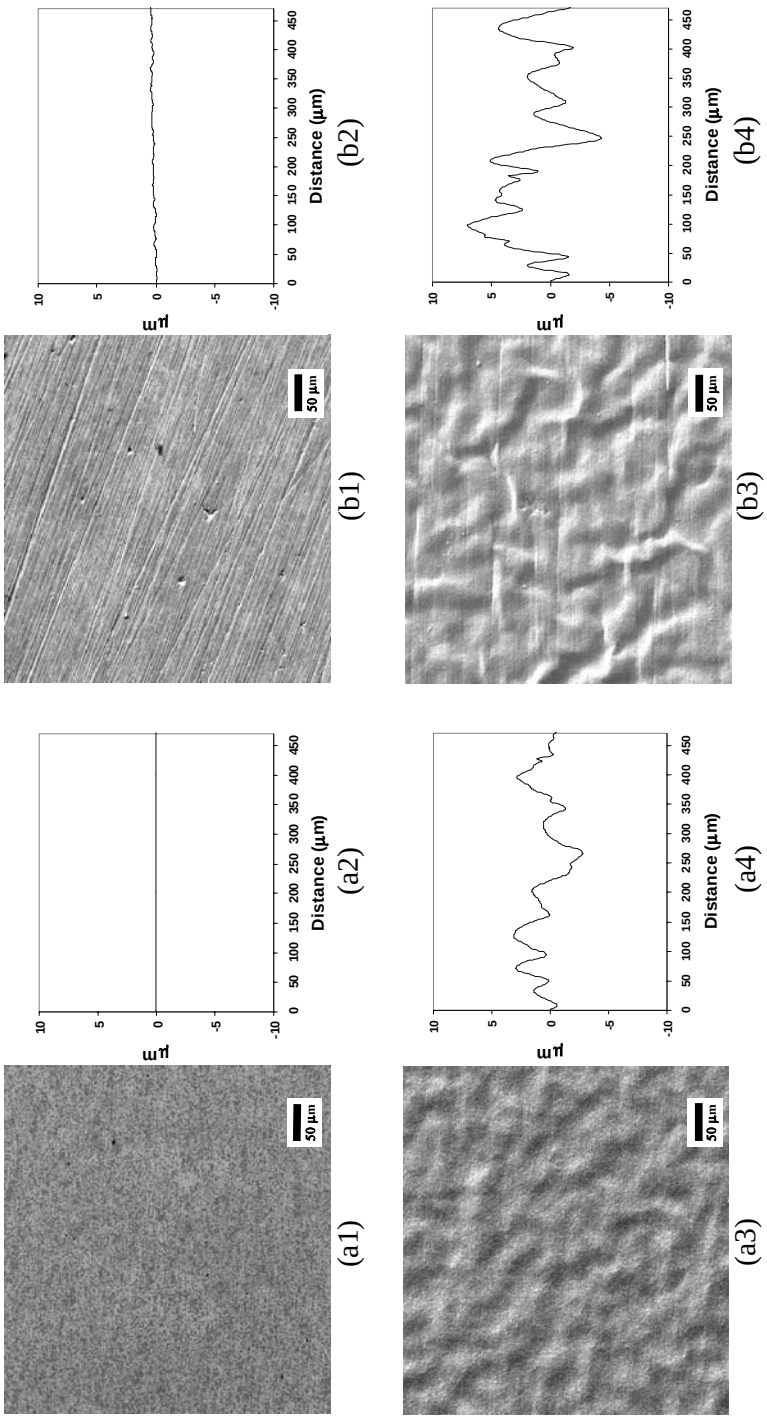

Figure 2: Representative SEM micrographs of initial and rumpled surfaces along with the corresponding profilometer scans for platinum aluminide BC. The SEM pictures and scans in a,b,c,d show BC surfaces polished successively down to 1 μm diamond paste, polished with 600 grit SiC paper, polished with 60 grit SiC paper and in an as-deposited condition, respectively. The profilometer scans in (a2,b2,c2,d2,a4,b4,c4,d4) correspond to the BC surfaces shown in (a1,b1,c1,d1,a3,b3,c3,d3), respectively. The Figs. (a1,b1,c1,d1) show BC surfaces before thermal cycling. After 25 thermal cycles, these surfaces become rumpled as shown in (a3,b3,c3,d3), respectively.

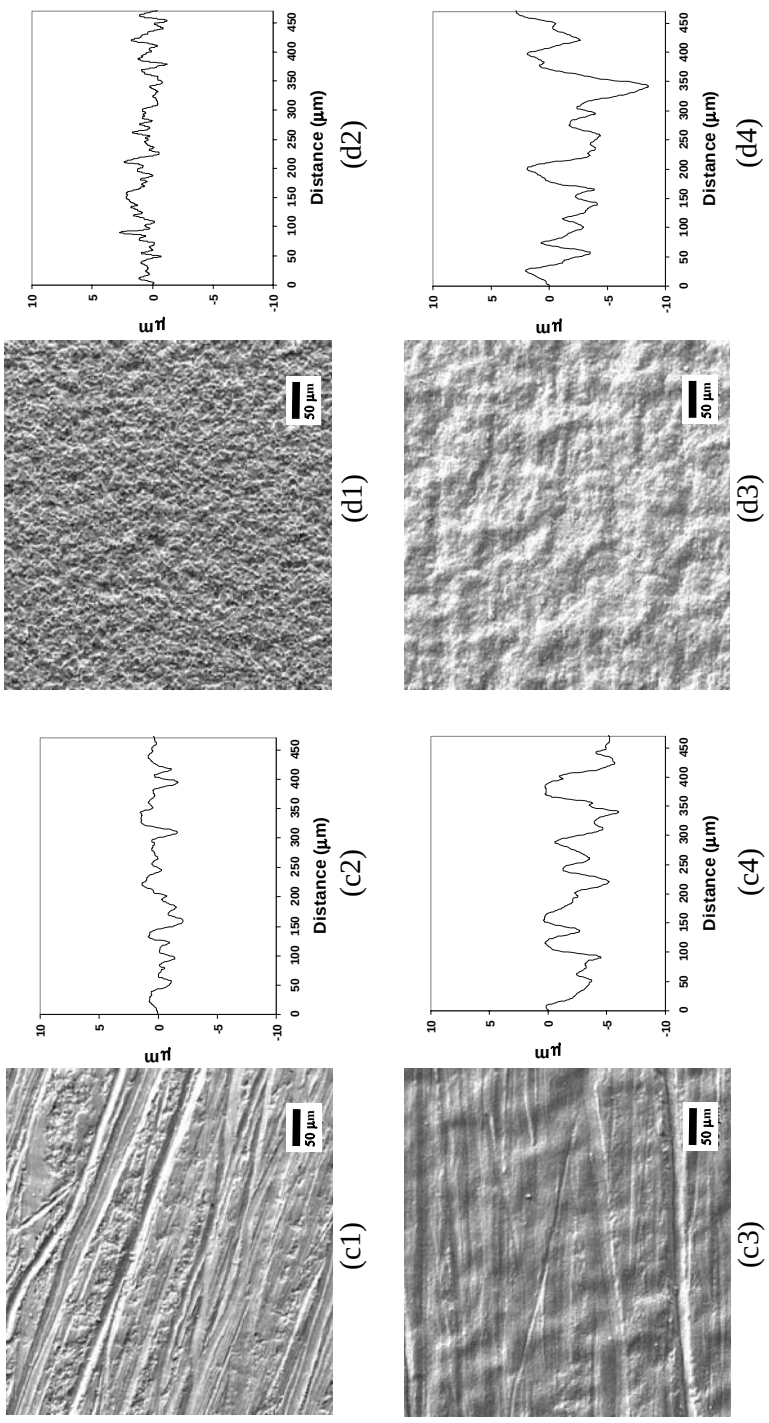

Figure 2: continued...

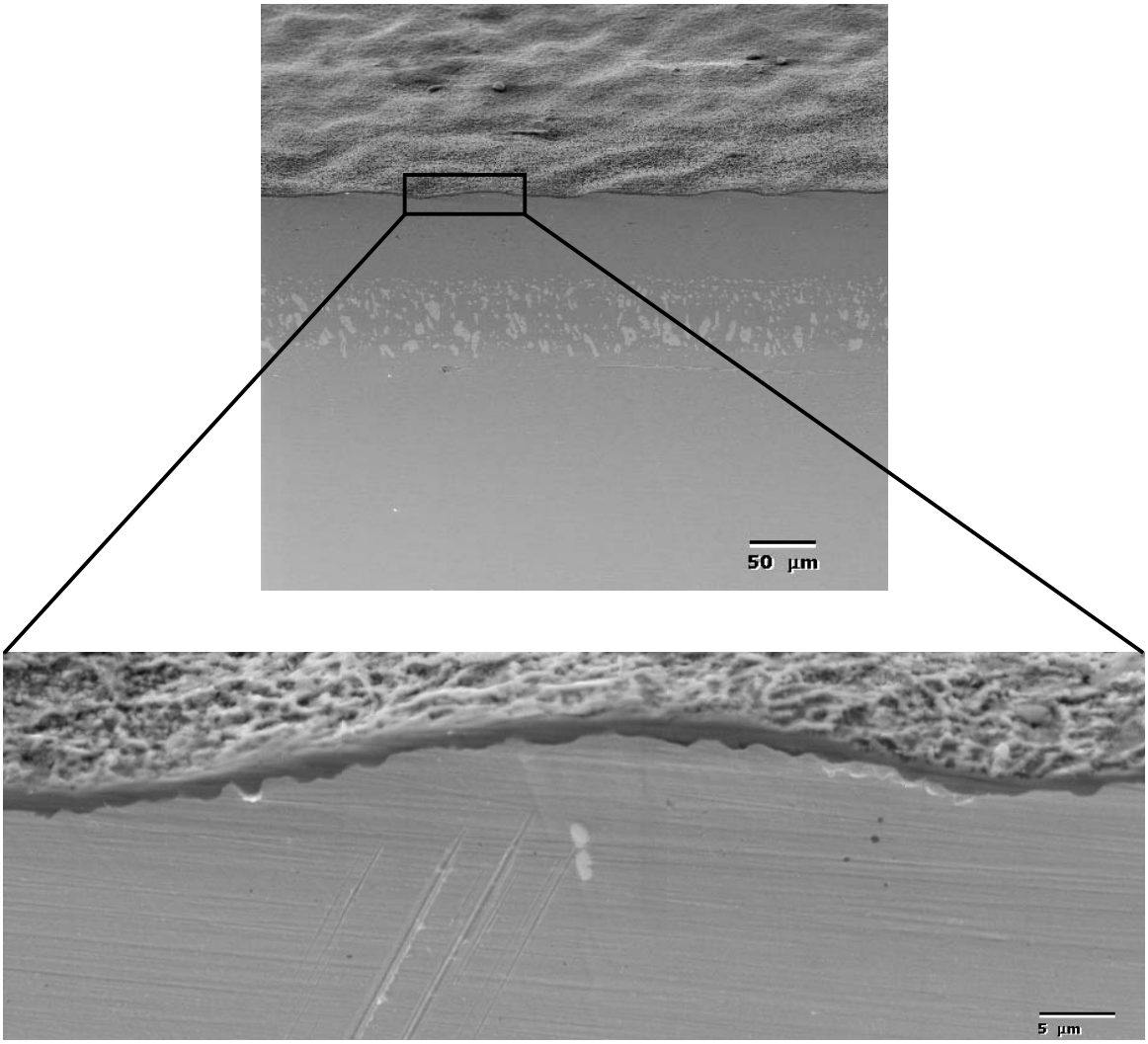

Figure 3: Scanning electron micrograph showing the TGO morphology formed after 25 thermal cycles on the platinum aluminide BC having an initial surface polished down to 1 μm diamond paste. The micrograph is taken at a tilt of 30° to the BC cross section.

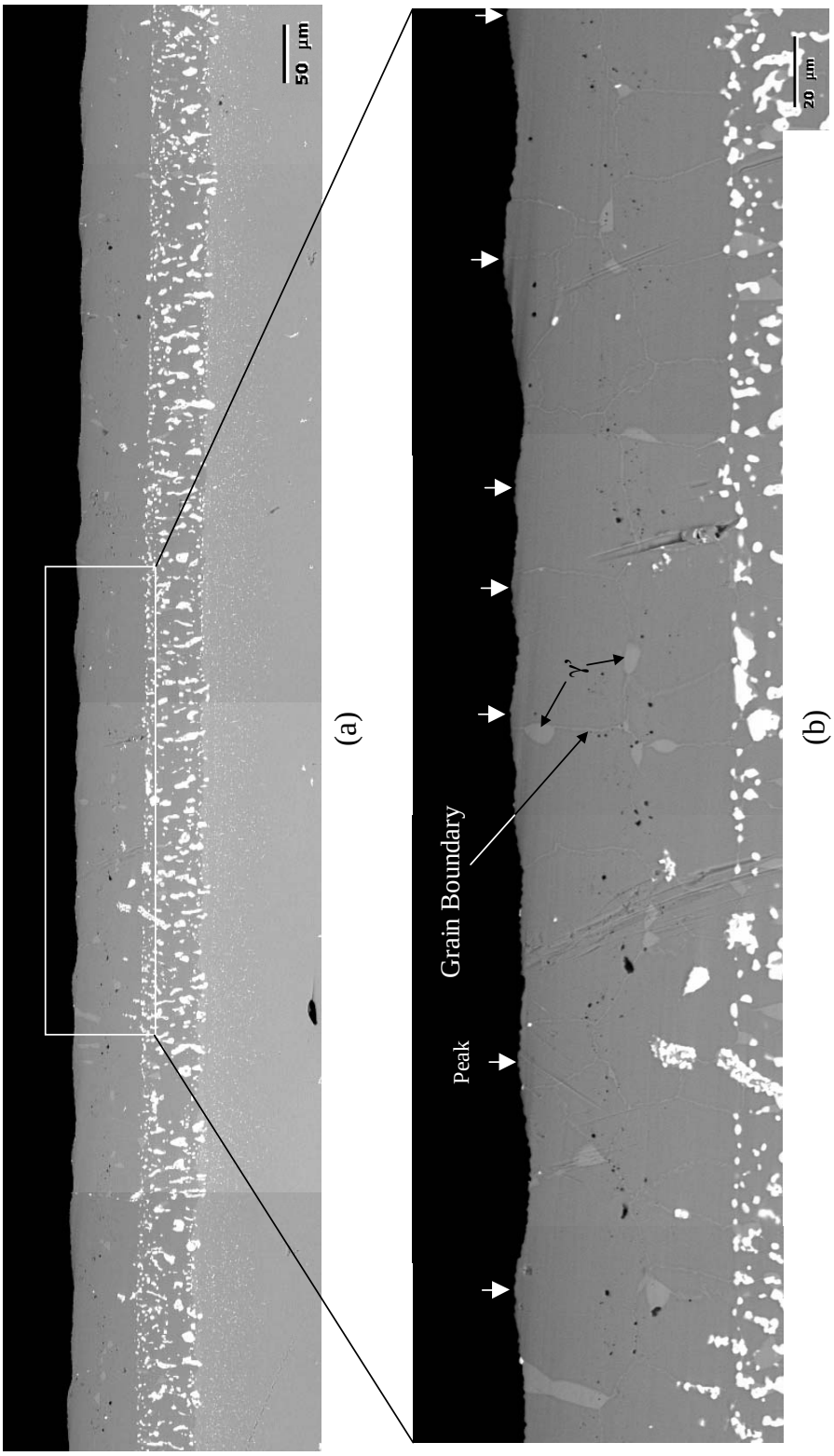

Figure 4: (a) Representative SEM micrograph (with backscatter electrons) of BC cross section showing the microstructure after 25 thermal cycles. (b) A close-up view shows γ' domains along with BC grain boundaries. The white arrows indicate peaks of rumples.

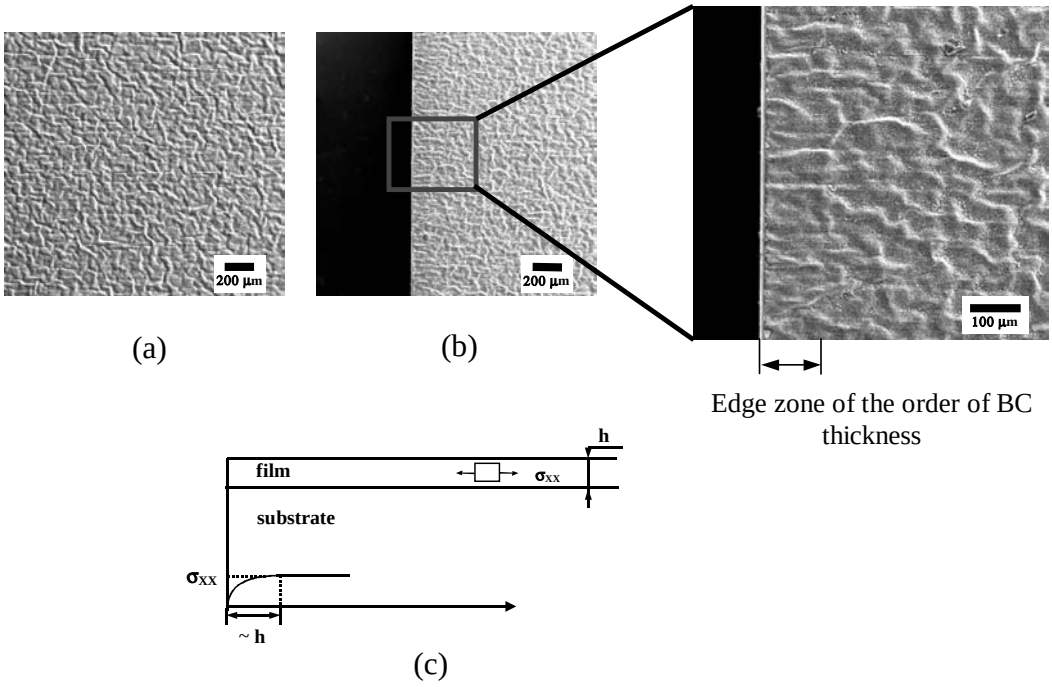

Figure 5: Rumpling at the (a) specimen center and (b) at the specimen edge. (c) Expected variation of the thermal mismatch stress in a thin film.

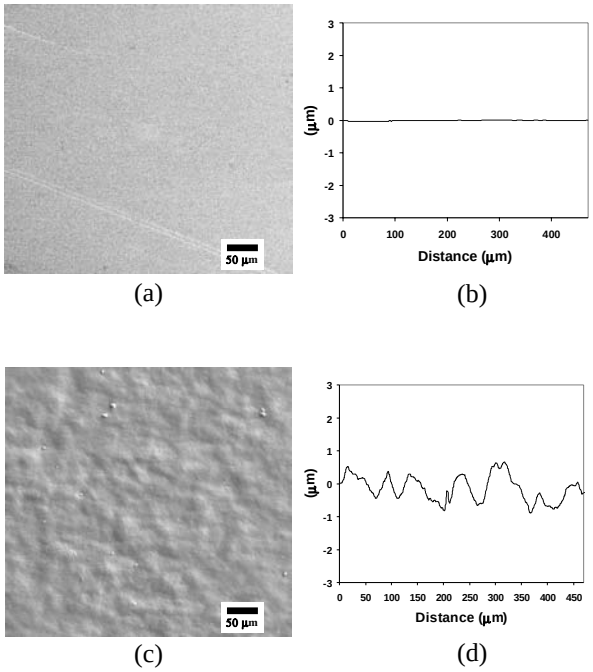

Figure 6: Representative SEM micrographs showing the top view of the NiCoCrAlY BC and corresponding profilometer scans. (a,b) Before thermal cycling, (c,d) After thermal cycling.

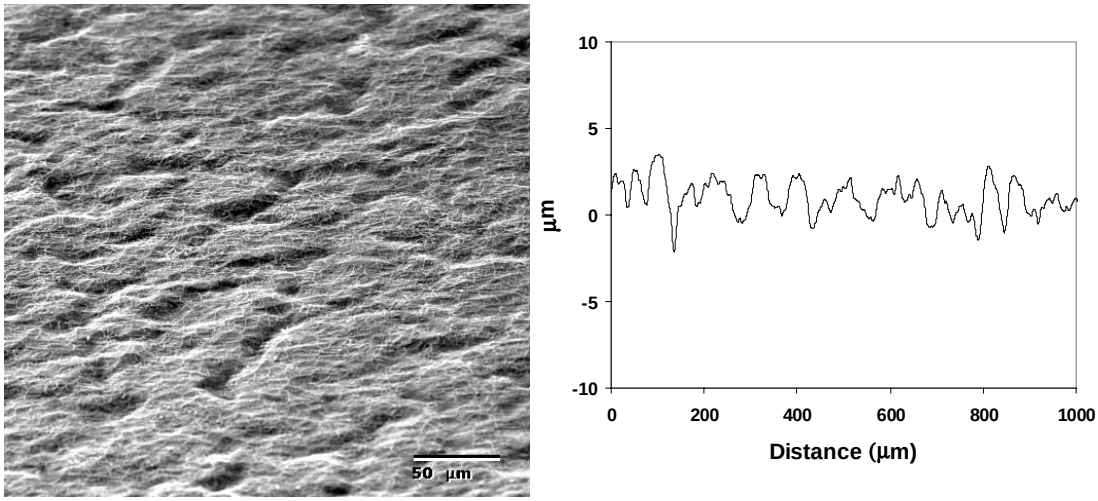

Figure 7: Top surface of platinum aluminide BC after 25 hour exposure at 1200 °C. (a) SEM micrograph taken at 30° inclination to the cross section, (b) profilometer scan.

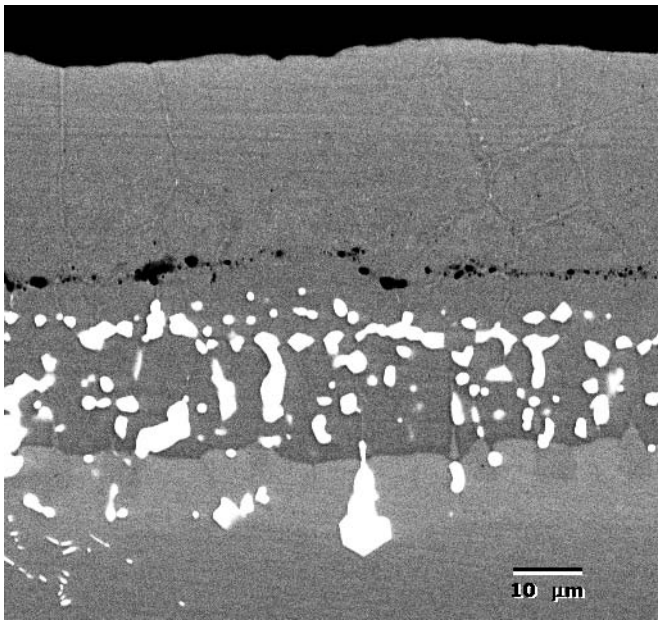

Figure 8: Representative SEM micrograph (with backscatter electrons) of platinum aluminide BC cross section showing the microstructure after 25 hour isothermal exposure at 1200 °C. Alumina inclusions can be seen as the dark regions at the boundary of the outer and the inner region of the BC. These alumina inclusions were present before the isothermal exposure (Fig. 1a).

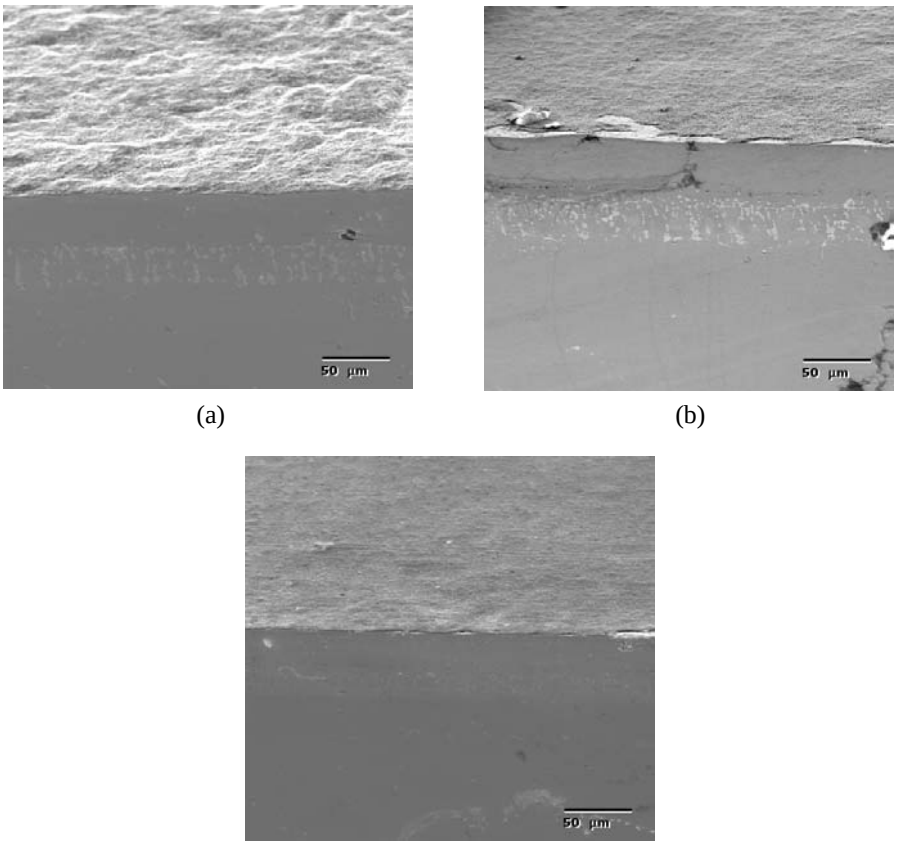

(a) (b)

(c)

Figure 9: Scanning electron micrographs of Platinum aluminide BC after isothermal exposure for 100 hours at (a) 1175 °C, (d) 1100 °C, and (e) 960 °C. The micrographs are taken at a tilt of 30° to the BC cross section.

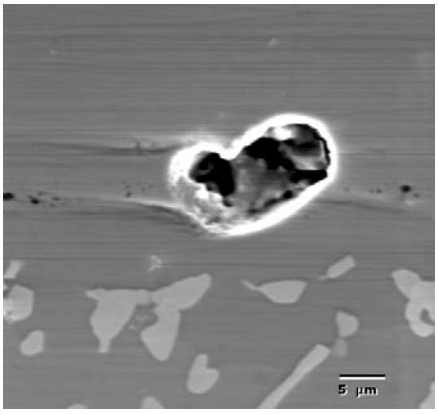

Figure 10: Scanning electron micrograph showing an isolated void formed in Platinum aluminide BC after 100 hour isothermal exposure at 1175 °C.

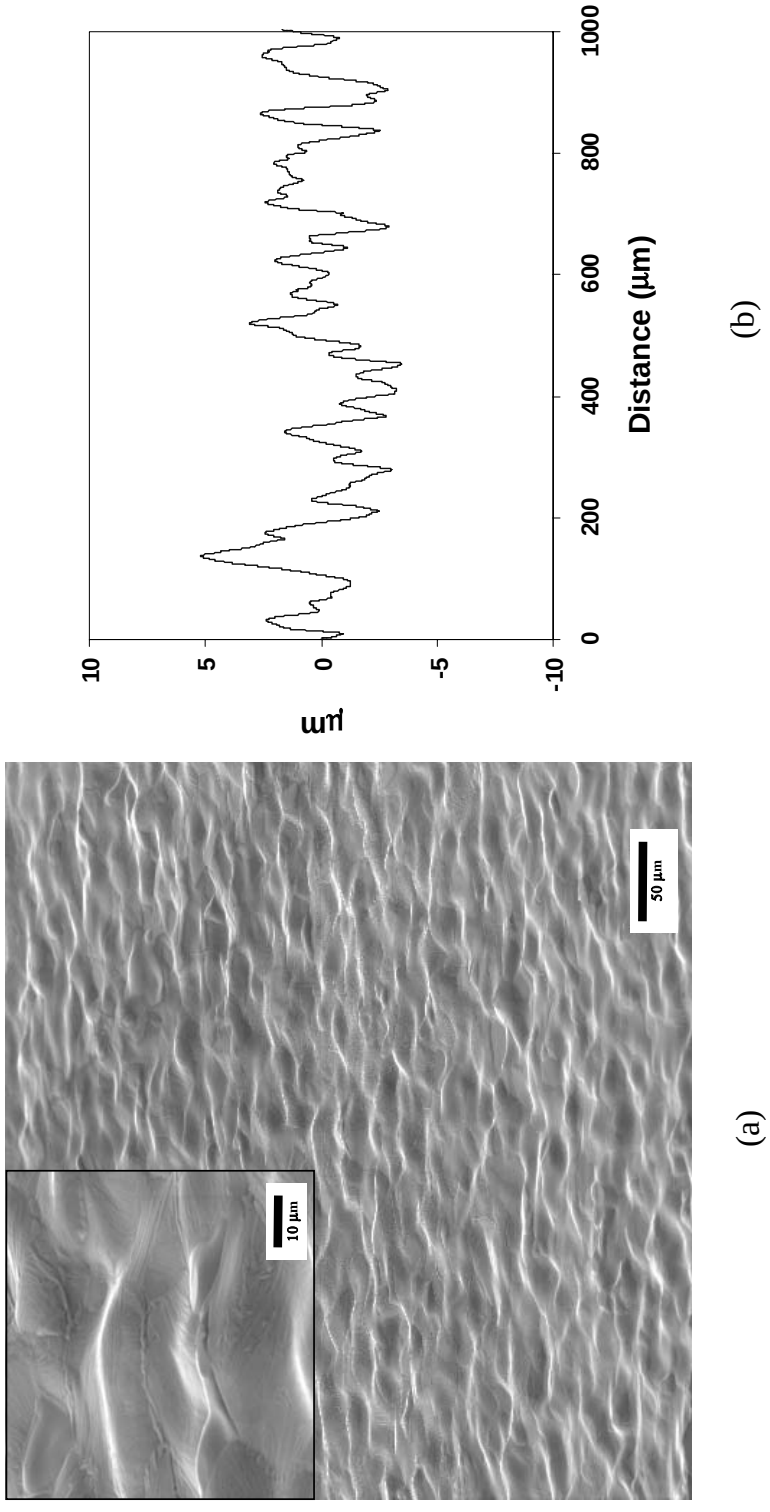

Figure 11: Platinum aluminide BC after 25 hour isothermal exposure at 1200 °C in vacuum. (a) SEM micrograph showing BC surface rumpling, (b) corresponding profilometer scan. The micrograph is taken at a tilt of 30° to the BC cross section.

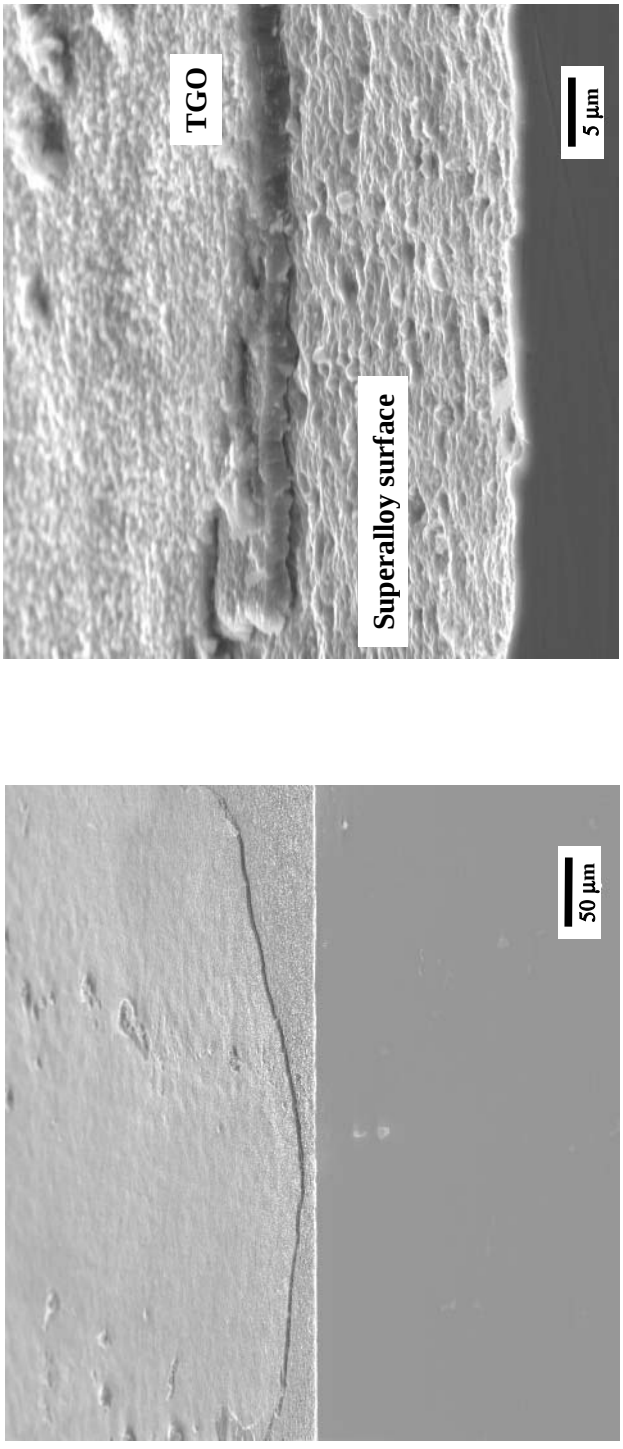

Figure 12: (a) Scanning electron micrograph showing an unrumpled surface of bulk superalloy after thermal cycling. (b) A close-up view showing superalloy surface that has developed roughness during thermal cycling. Prior to thermal cycling, the superalloy surface was polished successively down to 1 μm diamond paste, similar to that in Fig. 2(a1,a2). The micrograph is taken at a tilt of 30° to the superalloy cross-section.

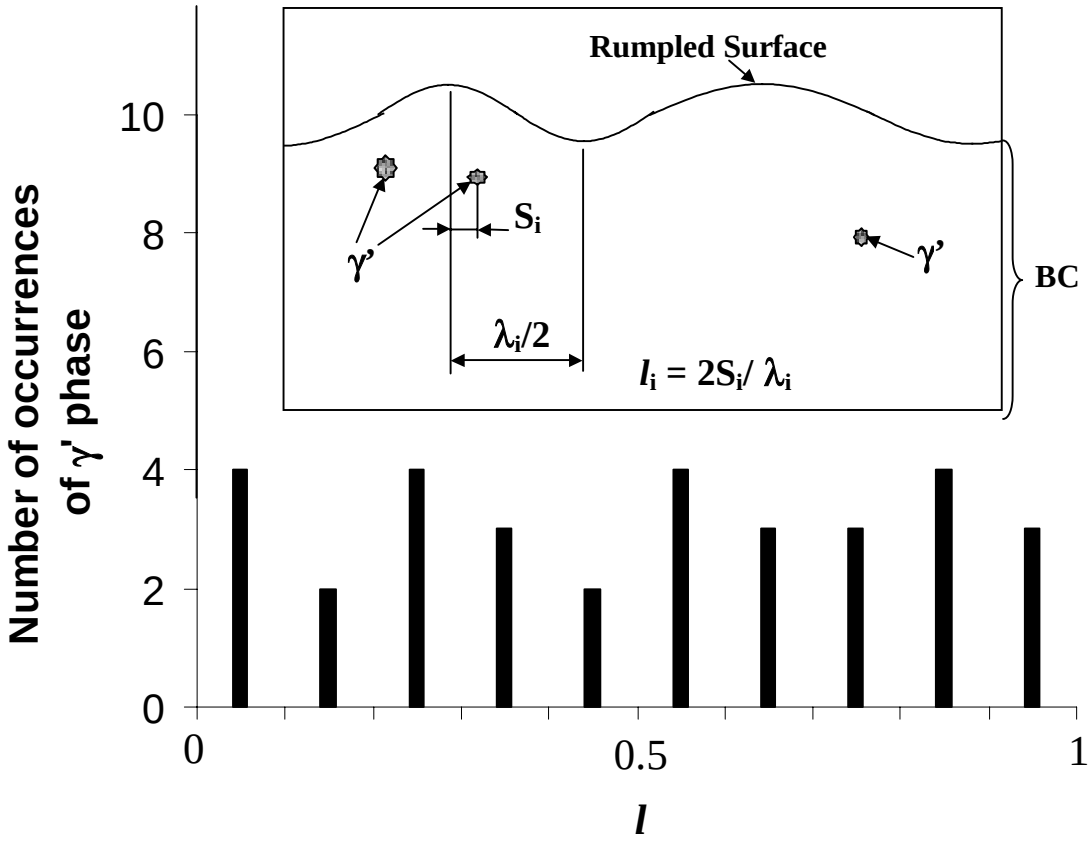

Figure 13: Occurrence of γ' phase relative to the rumples in Fig. 4. The schematic in the insert shows the method of calculating the γ' phase occurrence with respect to the rumpled surface.

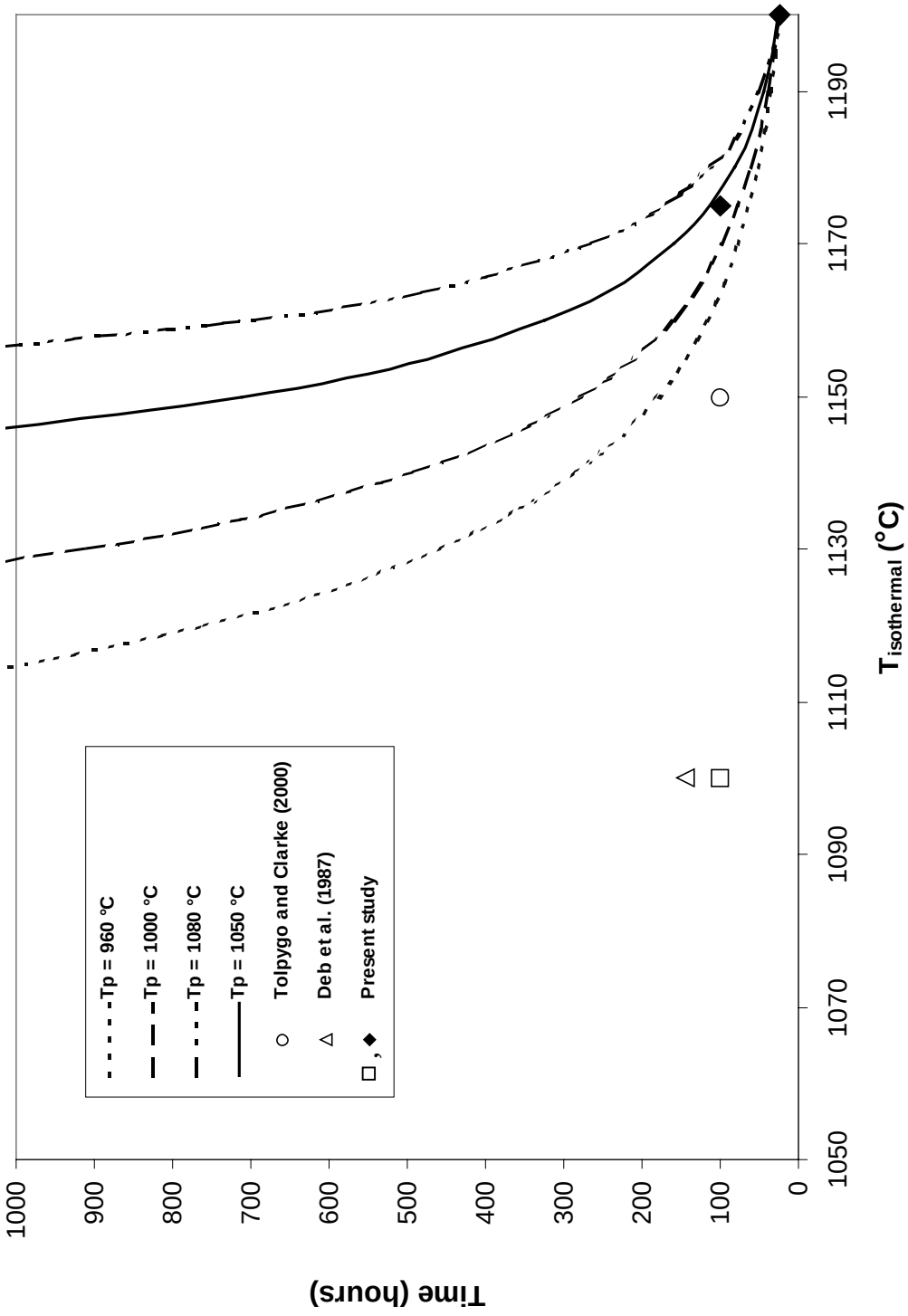

Figure 14: Time required to reach the comparable rumpling amplitude as that at 1200 °C after 25 hours for different processing temperatures based on the BC stress driven surface diffusion model by Panat *et al.* (2003). The open symbols indicate that BC rumpling did not occur, while the filled symbols indicate that BC rumpling occurred.

List of Recent TAM Reports

No.	Authors	Title	Date
938	Bagchi, P., and S. Balachandar	Linearly varying ambient flow past a sphere at finite Reynolds number—Part 1: Wake structure and forces in steady straining flow	Apr. 2000
939	Gioia, G., A. DeSimone, M. Ortiz, and A. M. Cuitiño	Folding energetics in thin-film diaphragms—*Proceedings of the Royal Society of London A* **458**, 1223–1229 (2002)	Apr. 2000
940	Chaïeb, S., and G. H. McKinley	Mixing immiscible fluids: Drainage induced cusp formation	May 2000
941	Thoroddsen, S. T., and A. Q. Shen	Granular jets—*Physics of Fluids* **13**, 4–6 (2001)	May 2000
942	Riahi, D. N.	Non-axisymmetric chimney convection in a mushy layer under a high-gravity environment—In *Centrifugal Materials Processing* (L. L. Regel and W. R. Wilcox, eds.), 295–302 (2001)	May 2000
943	Christensen, K. T., S. M. Soloff, and R. J. Adrian	PIV Sleuth: Integrated particle image velocimetry interrogation/validation software	May 2000
944	Wang, J., N. R. Sottos, and R. L. Weaver	Laser induced thin film spallation—*Experimental Mechanics* (submitted)	May 2000
945	Riahi, D. N.	Magnetohydrodynamic effects in high gravity convection during alloy solidification—In *Centrifugal Materials Processing* (L. L. Regel and W. R. Wilcox, eds.), 317–324 (2001)	June 2000
946	Gioia, G., Y. Wang, and A. M. Cuitiño	The energetics of heterogeneous deformation in open-cell solid foams—*Proceedings of the Royal Society of London A* **457**, 1079–1096 (2001)	June 2000
947	Kessler, M. R., and S. R. White	Self-activated healing of delamination damage in woven composites—*Composites A: Applied Science and Manufacturing* **32**, 683–699 (2001)	June 2000
948	Phillips, W. R. C.	On the pseudomomentum and generalized Stokes drift in a spectrum of rotational waves—*Journal of Fluid Mechanics* **430**, 209–229 (2001)	July 2000
949	Hsui, A. T., and D. N. Riahi	Does the Earth's nonuniform gravitational field affect its mantle convection?—*Physics of the Earth and Planetary Interiors* (submitted)	July 2000
950	Phillips, J. W.	Abstract Book, 20th International Congress of Theoretical and Applied Mechanics (27 August – 2 September, 2000, Chicago)	July 2000
951	Vainchtein, D. L., and H. Aref	Morphological transition in compressible foam—*Physics of Fluids* **13**, 2152–2160 (2001)	July 2000
952	Chaïeb, S., E. Sato-Matsuo, and T. Tanaka	Shrinking-induced instabilities in gels	July 2000
953	Riahi, D. N., and A. T. Hsui	A theoretical investigation of high Rayleigh number convection in a nonuniform gravitational field—*International Journal of Pure and Applied Mathematics*, in press (2003)	Aug. 2000
954	Riahi, D. N.	Effects of centrifugal and Coriolis forces on a hydromagnetic chimney convection in a mushy layer—*Journal of Crystal Growth* **226**, 393–405 (2001)	Aug. 2000
955	Fried, E.	An elementary molecular-statistical basis for the Mooney and Rivlin–Saunders theories of rubber-elasticity—*Journal of the Mechanics and Physics of Solids* **50**, 571–582 (2002)	Sept. 2000
956	Phillips, W. R. C.	On an instability to Langmuir circulations and the role of Prandtl and Richardson numbers—*Journal of Fluid Mechanics* **442**, 335–358 (2001)	Sept. 2000
957	Chaïeb, S., and J. Sutin	Growth of myelin figures made of water soluble surfactant—Proceedings of the 1st Annual International IEEE–EMBS Conference on Microtechnologies in Medicine and Biology (October 2000, Lyon, France), 345–348	Oct. 2000
958	Christensen, K. T., and R. J. Adrian	Statistical evidence of hairpin vortex packets in wall turbulence—*Journal of Fluid Mechanics* **431**, 433–443 (2001)	Oct. 2000

List of Recent TAM Reports (cont'd)

No.	*Authors*	*Title*	*Date*
959	Kuznetsov, I. R., and D. S. Stewart	Modeling the thermal expansion boundary layer during the combustion of energetic materials—*Combustion and Flame*, in press (2001)	Oct. 2000
960	Zhang, S., K. J. Hsia, and A. J. Pearlstein	Potential flow model of cavitation-induced interfacial fracture in a confined ductile layer—*Journal of the Mechanics and Physics of Solids*, **50**, 549–569 (2002)	Nov. 2000
961	Sharp, K. V., R. J. Adrian, J. G. Santiago, and J. I. Molho	Liquid flows in microchannels—Chapter 6 of *CRC Handbook of MEMS* (M. Gad-el-Hak, ed.) (2001)	Nov. 2000
962	Harris, J. G.	Rayleigh wave propagation in curved waveguides—*Wave Motion* **36**, 425–441 (2002)	Jan. 2001
963	Dong, F., A. T. Hsui, and D. N. Riahi	A stability analysis and some numerical computations for thermal convection with a variable buoyancy factor—*Journal of Theoretical and Applied Mechanics* **2**, 19–46 (2002)	Jan. 2001
964	Phillips, W. R. C.	Langmuir circulations beneath growing or decaying surface waves—*Journal of Fluid Mechanics* (submitted)	Jan. 2001
965	Bdzil, J. B., D. S. Stewart, and T. L. Jackson	Program burn algorithms based on detonation shock dynamics—*Journal of Computational Physics* (submitted)	Jan. 2001
966	Bagchi, P., and S. Balachandar	Linearly varying ambient flow past a sphere at finite Reynolds number: Part 2—Equation of motion—*Journal of Fluid Mechanics* (submitted)	Feb. 2001
967	Cermelli, P., and E. Fried	The evolution equation for a disclination in a nematic fluid—*Proceedings of the Royal Society A* **458**, 1–20 (2002)	Apr. 2001
968	Riahi, D. N.	Effects of rotation on convection in a porous layer during alloy solidification—Chapter 12 in *Transport Phenomena in Porous Media* (D. B. Ingham and I. Pop, eds.), 316–340 (2002)	Apr. 2001
969	Damljanovic, V., and R. L. Weaver	Elastic waves in cylindrical waveguides of arbitrary cross section—*Journal of Sound and Vibration* (submitted)	May 2001
970	Gioia, G., and A. M. Cuitiño	Two-phase densification of cohesive granular aggregates—*Physical Review Letters* **88**, 204302 (2002) (in extended form and with added co-authors S. Zheng and T. Uribe)	May 2001
971	Subramanian, S. J., and P. Sofronis	Calculation of a constitutive potential for isostatic powder compaction—*International Journal of Mechanical Sciences* (submitted)	June 2001
972	Sofronis, P., and I. M. Robertson	Atomistic scale experimental observations and micromechanical/continuum models for the effect of hydrogen on the mechanical behavior of metals—*Philosophical Magazine* (submitted)	June 2001
973	Pushkin, D. O., and H. Aref	Self-similarity theory of stationary coagulation—*Physics of Fluids* **14**, 694–703 (2002)	July 2001
974	Lian, L., and N. R. Sottos	Stress effects in ferroelectric thin films—*Journal of the Mechanics and Physics of Solids* (submitted)	Aug. 2001
975	Fried, E., and R. E. Todres	Prediction of disclinations in nematic elastomers—*Proceedings of the National Academy of Sciences* **98**, 14773–14777 (2001)	Aug. 2001
976	Fried, E., and V. A. Korchagin	Striping of nematic elastomers—*International Journal of Solids and Structures* **39**, 3451–3467 (2002)	Aug. 2001
977	Riahi, D. N.	On nonlinear convection in mushy layers: Part I. Oscillatory modes of convection—*Journal of Fluid Mechanics* **467**, 331–359 (2002)	Sept. 2001
978	Sofronis, P., I. M. Robertson, Y. Liang, D. F. Teter, and N. Aravas	Recent advances in the study of hydrogen embrittlement at the University of Illinois—Invited paper, Hydrogen–Corrosion Deformation Interactions (Sept. 16–21, 2001, Jackson Lake Lodge, Wyo.)	Sept. 2001
979	Fried, E., M. E. Gurtin, and K. Hutter	A void-based description of compaction and segregation in flowing granular materials—*Proceedings of the Royal Society of London A* (submitted)	Sept. 2001

List of Recent TAM Reports (cont'd)

No.	Authors	Title	Date
980	Adrian, R. J., S. Balachandar, and Z.-C. Liu	Spanwise growth of vortex structure in wall turbulence—*Korean Society of Mechanical Engineers International Journal* **15**, 1741–1749 (2001)	Sept. 2001
981	Adrian, R. J.	Information and the study of turbulence and complex flow—*Japanese Society of Mechanical Engineers Journal B*, in press (2002)	Oct. 2001
982	Adrian, R. J., and Z.-C. Liu	Observation of vortex packets in direct numerical simulation of fully turbulent channel flow—*Journal of Visualization*, in press (2002)	Oct. 2001
983	Fried, E., and R. E. Todres	Disclinated states in nematic elastomers—*Journal of the Mechanics and Physics of Solids* **50**, 2691–2716 (2002)	Oct. 2001
984	Stewart, D. S.	Towards the miniaturization of explosive technology—Proceedings of the 23rd International Conference on Shock Waves (2001)	Oct. 2001
985	Kasimov, A. R., and Stewart, D. S.	Spinning instability of gaseous detonations—*Journal of Fluid Mechanics* (submitted)	Oct. 2001
986	Brown, E. N., N. R. Sottos, and S. R. White	Fracture testing of a self-healing polymer composite—*Experimental Mechanics* (submitted)	Nov. 2001
987	Phillips, W. R. C.	Langmuir circulations—*Surface Waves* (J. C. R. Hunt and S. Sajjadi, eds.), in press (2002)	Nov. 2001
988	Gioia, G., and F. A. Bombardelli	Scaling and similarity in rough channel flows—*Physical Review Letters* **88**, 014501 (2002)	Nov. 2001
989	Riahi, D. N.	On stationary and oscillatory modes of flow instabilities in a rotating porous layer during alloy solidification—*Journal of Porous Media*, in press (2002)	Nov. 2001
990	Okhuysen, B. S., and D. N. Riahi	Effect of Coriolis force on instabilities of liquid and mushy regions during alloy solidification—*Physics of Fluids* (submitted)	Dec. 2001
991	Christensen, K. T., and R. J. Adrian	Measurement of instantaneous Eulerian acceleration fields by particle-image accelerometry: Method and accuracy—*Experimental Fluids* (submitted)	Dec. 2001
992	Liu, M., and K. J. Hsia	Interfacial cracks between piezoelectric and elastic materials under in-plane electric loading—*Journal of the Mechanics and Physics of Solids* **51**, 921–944 (2003)	Dec. 2001
993	Panat, R. P., S. Zhang, and K. J. Hsia	Bond coat surface rumpling in thermal barrier coatings—*Acta Materialia* **51**, 239–249 (2003)	Jan. 2002
994	Aref, H.	A transformation of the point vortex equations—*Physics of Fluids* **14**, 2395–2401 (2002)	Jan. 2002
995	Saif, M. T. A, S. Zhang, A. Haque, and K. J. Hsia	Effect of native Al_2O_3 on the elastic response of nanoscale aluminum films—*Acta Materialia* **50**, 2779–2786 (2002)	Jan. 2002
996	Fried, E., and M. E. Gurtin	A nonequilibrium theory of epitaxial growth that accounts for surface stress and surface diffusion—*Journal of the Mechanics and Physics of Solids*, in press (2002)	Jan. 2002
997	Aref, H.	The development of chaotic advection—*Physics of Fluids* **14**, 1315–1325 (2002); see also *Virtual Journal of Nanoscale Science and Technology*, 11 March 2002	Jan. 2002
998	Christensen, K. T., and R. J. Adrian	The velocity and acceleration signatures of small-scale vortices in turbulent channel flow—*Journal of Turbulence*, in press (2002)	Jan. 2002
999	Riahi, D. N.	Flow instabilities in a horizontal dendrite layer rotating about an inclined axis—*Proceedings of the Royal Society of London A* (submitted)	Feb. 2002
1000	Kessler, M. R., and S. R. White	Cure kinetics of ring-opening metathesis polymerization of dicyclopentadiene—*Journal of Polymer Science A* **40**, 2373–2383 (2002)	Feb. 2002
1001	Dolbow, J. E., E. Fried, and A. Q. Shen	Point defects in nematic gels: The case for hedgehogs—*Proceedings of the National Academy of Sciences* (submitted)	Feb. 2002
1002	Riahi, D. N.	Nonlinear steady convection in rotating mushy layers—*Journal of Fluid Mechanics*, in press (2003)	Mar. 2002

List of Recent TAM Reports (cont'd)

No.	*Authors*	*Title*	*Date*
1003	Carlson, D. E., E. Fried, and S. Sellers	The totality of soft-states in a neo-classical nematic elastomer—*Proceedings of the Royal Society A* (submitted)	Mar. 2002
1004	Fried, E., and R. E. Todres	Normal-stress differences and the detection of disclinations in nematic elastomers—*Journal of Polymer Science B: Polymer Physics* **40**, 2098–2106 (2002)	June 2002
1005	Fried, E., and B. C. Roy	Gravity-induced segregation of cohesionless granular mixtures—*Lecture Notes in Mechanics*, in press (2002)	July 2002
1006	Tomkins, C. D., and R. J. Adrian	Spanwise structure and scale growth in turbulent boundary layers—*Journal of Fluid Mechanics* (submitted)	Aug. 2002
1007	Riahi, D. N.	On nonlinear convection in mushy layers: Part 2. Mixed oscillatory and stationary modes of convection—*Journal of Fluid Mechanics* (submitted)	Sept. 2002
1008	Aref, H., P. K. Newton, M. A. Stremler, T. Tokieda, and D. L. Vainchtein	Vortex crystals—*Advances in Applied Mathematics* **39**, in press (2002)	Oct. 2002
1009	Bagchi, P., and S. Balachandar	Effect of turbulence on the drag and lift of a particle—*Physics of Fluids* (submitted)	Oct. 2002
1010	Zhang, S., R. Panat, and K. J. Hsia	Influence of surface morphology on the adhesive strength of aluminum/epoxy interfaces—*Journal of Adhesion Science and Technology* (submitted)	Oct. 2002
1011	Carlson, D. E., E. Fried, and D. A. Tortorelli	On internal constraints in continuum mechanics—*Journal of Elasticity* (submitted)	Oct. 2002
1012	Boyland, P. L., M. A. Stremler, and H. Aref	Topological fluid mechanics of point vortex motions—*Physica D* **175**, 69–95 (2002)	Oct. 2002
1013	Bhattacharjee, P., and D. N. Riahi	Computational studies of the effect of rotation on convection during protein crystallization—*Journal of Crystal Growth* (submitted)	Feb. 2003
1014	Brown, E. N., M. R. Kessler, N. R. Sottos, and S. R. White	*In situ* poly(urea-formaldehyde) microencapsulation of dicyclopentadiene—*Journal of Microencapsulation* (submitted)	Feb. 2003
1015	Brown, E. N., S. R. White, and N. R. Sottos	Microcapsule induced toughening in a self-healing polymer composite—*Journal of Materials Science* (submitted)	Feb. 2003
1016	Kuznetsov, I. R., and D. S. Stewart	Burning rate of energetic materials with thermal expansion—*Combustion and Flame* (submitted)	Mar. 2003
1017	Dolbow, J., E. Fried, and H. Ji	Chemically induced swelling of hydrogels—*Journal of the Mechanics and Physics of Solids* (submitted)	Mar. 2003
1018	Costello, G. A.	Mechanics of wire rope—Mordica Lecture, Interwire 2003, Wire Association International, Atlanta, Georgia, May 12, 2003	Mar. 2003
1019	Wang, J., N. R. Sottos, and R. L. Weaver	Thin film adhesion measurement by laser induced stress waves—*Journal of the Mechanics and Physics of Solids* (submitted)	Apr. 2003
1020	Bhattacharjee, P., and D. N. Riahi	Effect of rotation on surface tension driven flow during protein crystallization—*Microgravity Science and Technology* (submitted)	Apr. 2003
1021	Fried, E.	The configurational and standard force balances are not always statements of a single law—*Proceedings of the Royal Society* (submitted)	Apr. 2003
1022	Panat, R. P., and K. J. Hsia	Experimental investigation of the bond coat rumpling instability under isothermal and cyclic thermal histories in thermal barrier systems—*Proceedings of the Royal Society of London A* (submitted)	May 2003